The Terrestrial Planet Finder Coronagraph Optical Surface Requirements

Stuart B. Shaklan[1], Joseph J. Green, David M. Palacios
Jet Propulsion Laboratory,
California Institute of Technology

ABSTRACT

We derive the requirements on the surface height uniformity and reflectivity uniformity of the Terrestrial Planet Finder Coronagraph telescope and instrument optics for spatial frequencies within and beyond the spatial control bandwidth of the wave front control system. Three different wave front control systems are considered: a zero-path difference Michelson interferometer with two deformable mirrors at a pupil image; a sequential pair of deformable mirrors with one placed at a pupil image; and the Visible Nuller spatially-filtered controller. We show that the optical bandwidth limits the useful outer working angle.

Keywords: coronagraph, high-contrast imaging, telescope requirements

1. INTRODUCTION

It is widely believed that the ultra-high-dynamic range imaging performance of the Terrestrial Planet Finder Coronagraph[1] (TPF-C) places extraordinarily tight requirements on the smoothness, accuracy, and reflectivity uniformity of its optical surfaces. In this paper, we show that the requirements depend on the optical bandwidth, beam diameter, propagation distance, spatial frequency, and the architecture of the wave front control system. We show that wave front control with the right combination of deformable mirrors (DMs) relaxes the optical requirements to within the existing state-of-the-art, over a finite field of regard. Our results apply to the entire optical system from the telescope primary mirror to the coronagraph optics that image starlight onto the coronagraph mask. In particular, we find that the primary and secondary mirrors do not require extraordinary surface figure or reflectivity uniformity.

We begin by reviewing the derivation by Shaklan & Green (2006) of the propagation of light through the TPF-C optical train[2]. This work considered spatial frequencies within the control bandpass of the DMs. We showed how two wave front control systems – the Michelson[3] and the sequential DM configurations – exhibit wavelength dependencies that partially compensate the wavelength dependence of surface height and reflectivity uniformity in the system. The sequential DM configuration provides broad-band compensation of reflectivity nonuniformities. It substantially relaxes the amplitude uniformity and surface height requirements relative to the Michelson controller. In this paper, we extend our earlier analysis to the Visible Nuller[4] coronagraph and show that its wave front control system has the same broadband dependency as the Michelson configuration.

Here we also address the scatter of high spatial frequencies – those frequencies beyond the DM spatial control bandwidth. These spatial frequencies beat together and scatter light into the coronagraph 'dark hole' generating speckles whose amplitude varies as the inverse square of wavelength. We derive the limitations of the Michelson and sequential configuration in compensating the wavelength dependence of this light and show that current optical fabrication technology leads to acceptable levels of the frequency folding effect.

We conclude this paper with an important result: *the maximum dimension of the dark hole is limited by the optical bandpass.* We show that for a 100 nm bandpass, , the optical surface quality required to mitigate this effect far exceeds the state-of-the art in optical fabrication beyond 20 cycles/aperture for the Michelson and Visible Nuller controllers and ~ 30 cycles/aperture for the sequential configuration. While some rearrangement of the optical train helps to relax the

[1] Contact information: Address: 4800 Oak Grove Drive, Pasadena, CA 91109. e-mail: Stuart.Shaklan@jpl.nasa.gov

surface requirements, the problem is constrained by the need to reimage pupils on the scale of a few cm, fold the beam on a scale of a few meters, and form images where coronagraph masks can be placed.

2. REVIEW OF PROPAGATION IN THE TPF-C OPTICAL TRAIN

TPF-C is a proposed large, ultra-stable, orbiting optical telescope that works with a coronagraph and a wave front control system to reduce diffracted and scattered light to levels below 10^{-10} in close proximity to the image of a target star. At these low light levels, TPF-C can detect the light reflected from Earth-like planets in orbits where liquid water could exist[5]. The optical system layout up to the coronagraph entrance pupil is depicted in Fig. 1.

The primary mirror (PM) is imaged onto the coarse deformable mirror (CDM). These serve as the entrance pupil and system stop. (The CDM is actually conjugate to the downstream fine DM and the coronagraph Lyot plane, which ultimately limits the beam shape.) The beam is collimated to a 10 cm diameter at the CDM and remains 10 cm throughout the coronagraph optical train except where image planes are required (not shown). This diameter is matched to the size of a 100 x 100 element deformable mirror made by Xinetics[6], a larger version of the DMs currently used in the TPF-C High Contrast Imaging Testbed[7]. A cylindrical telescope formed by anamorphic optics Cyl1 and Cyl2 reshapes the elliptical beam formed by the 8 x 3.5 m primary into a circular beam at the CDM.

When viewed from the CDM, the images of all the optics are 10 cm in diameter. The image of the PM is superimposed on the CDM, and the secondary mirror (SM) image is just 8.35 cm away. The two optics closest to the telescope Cassegrain focus, fold mirrors M3 and M4, are imaged about 10 m away. The effective distance z between the image of each optic and the pupil plane where the CDM is located is available in reference 2. We note that the Fresnel number of the system, $F = D^2 / 4\lambda z$, where λ is the wavelength of the light and D is the beam diameter, is about F=500 in the visible for the longest propagation distance z=10.44 m. At F=500, the beam diffraction remains mostly plane wave in nature. We will ignore edge ringing throughout this paper.

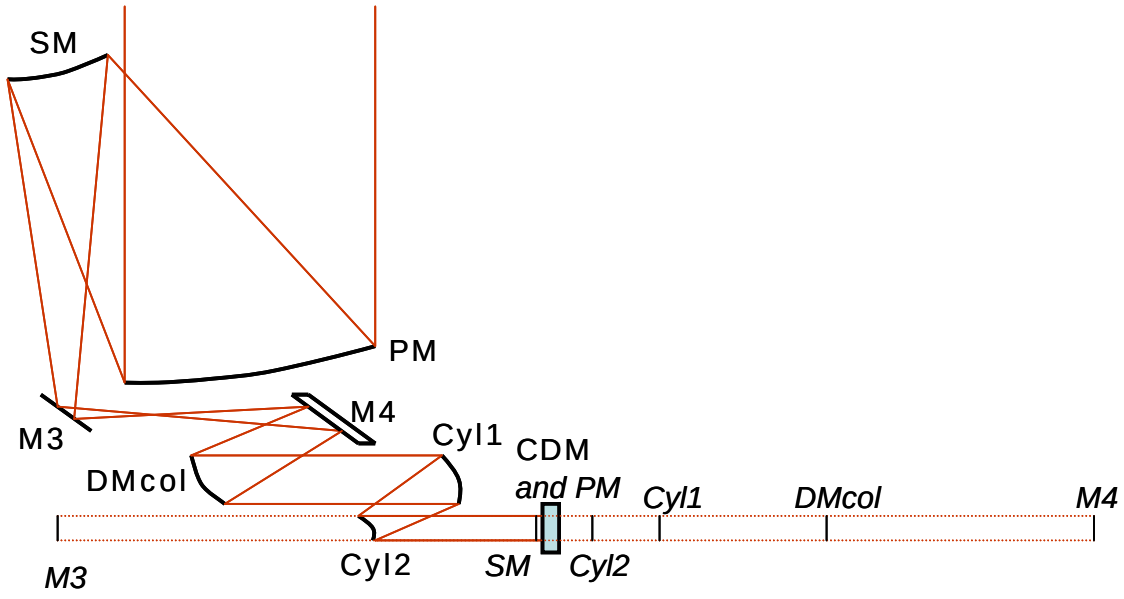

Figure 1. TPF optical layout up to the coarse DM (not to scale). Bold font: optics position. Italics: Image of the optic as seen from the coarse DM. PM: Primary Mirror. SM: Secondary Mirror. M3 and M4: flat fold mirrors. DMcol: Collimating mirror. Cyl1 and Cyl2: cylindrical telescope to circularize the beam. CDM: coarse DM. The PM is imaged onto the CDM. The beam is collimated to a 10 cm diameter at the CDM. Hence the images of all the optics are also 10 cm in diameter.

The optics are not ideal; they have spatial surface and reflectivity variations. Each optic modifies the phase and amplitude profile of the light propagating through the system. Fig. 2 shows what happens to the beam when it encounters a weak surface corrugation and reflectivity corrugation of N cycles/aperture. The beam splits into the undiffracted component and diffracted components at angles +/- $\theta=N\lambda/D$. Ultimately the light propagates to form an Airy spot in the image plane at $f\theta$, where f is the effective focal length. After a propagation distance z, the undiffracted and diffracted components have a relative delay given by $d = zN^2\lambda^2/(2D^2)$.

The coronagraph is designed to remove the undiffracted component. Any number of coronagraph designs can do this with high efficiency (e.g. band-limited Lyot[8], shaped-pupil[9], pupil remapping[10], and optical vortices[11] among others). From this point on, we only consider light in the diffracted component.

The phase of the diffracted component after propagating from a non-pupil plane to the pupil plane is given by $\phi=2\pi d/\lambda$ so that the electric field at the pupil is

$$E \approx \left[\frac{\sqrt{2} r_N}{2} \cos(2\pi yN/D + \psi) + i\sqrt{2}\alpha_N \cos(2\pi yN/D + \varphi_N) \right] e^{i\phi} \tag{1}$$

where α_N and r_N are the r.m.s. values of the wavefront phase and surface reflectivity, respectively, at N cycles/aperture. To arrive at Eq. 1, we have assumed that $\alpha << 1$ radian so that $e^{i\alpha} \sim 1+i\alpha$. Expanding $e^{i\phi}$, keeping terms to second order, and expressing the r.m.s. electric field in terms of the r.m.s. amplitude and phase, we arrive at

$$E = \left[\frac{r}{2}\left(1 - \frac{1}{2}\left(\frac{\pi z\lambda N^2}{D^2}\right)^2\right) - \frac{\alpha\pi z\lambda N^2}{D^2},\ \ \alpha\left(1 - \frac{1}{2}\left(\frac{\pi z\lambda N^2}{D^2}\right)^2\right) + \frac{\pi rz\lambda N^2}{2D^2} \right]. \tag{2}$$

We have used the notation [real, imaginary] to represent the complex field. We have also dropped the N-subscripts for notational simplicity. The reader should keep in mind that r and α refer to the r.m.s. fractional reflectivity and phase (in radians) at N cycles/aperture, averaged over a 1 cycle/aperture bandwidth (equivalent to one speckle in the image plane). The phase term α arises from a periodic piston of the mirror surface, $\alpha = 4\pi s/\lambda$, where s is the r.m.s. of the periodic surface deformation. Substituting into Eq. 2, we find that the residual electric field r.m.s. is

$$\begin{aligned} E &= \left[\frac{r}{2} - \frac{r}{4}\left(\frac{\pi z\lambda N^2}{D^2}\right)^2 - \frac{4\pi^2 szN^2}{D^2},\ \ \frac{4\pi s}{\lambda} - \frac{2\pi^3 sz^2\lambda N^4}{D^4} - \frac{\pi rz\lambda N^2}{2D^2} \right] \\ &= \left[E_r - E_{r,p2} - E_{s,p},\ \ E_s - E_{s,p2} - E_{r,p} \right] \\ &= \left[E_A, E_\phi \right] \end{aligned} \tag{3}$$

The first real term, E_r, describes the impact of amplitude non-uniformities of an optic. Assuming that spatial variations in r are uniform over the spectral band (a reasonable assumption for a metallic coating in a restricted optical band), the amplitude term E_r is independent of wavelength. The second term $E_{r,p2}$ accounts for the second-order propagation (the expansion of the cosine leading to Eq. 2) after the beam has propagated a distance z. The third real term, $E_{s,p}$, is called the phase-induced-amplitude and is the amplitude arising from the first order propagation of the surface non-uniformities s into amplitude non-uniformities at distance z.. We will show below that E_r and $E_{s,p}$ are perfectly compensated by the wavelength-independent amplitude created by the sequential DM configuration.

The imaginary term, E_s, is the phase in the pupil plane. The second imaginary term $E_{s,p2}$, is the second-order propagation of phase non-uniformities over a distance z. The third term $E_{r,p}$ is the amplitude-induced-phase. A DM in the pupil can compensate for E_s, but the linear wavelength dependence of $E_{s,p2}$ and $E_{r,p}$ is not fully controllable in broad-band light using any of the DM configurations under consideration.

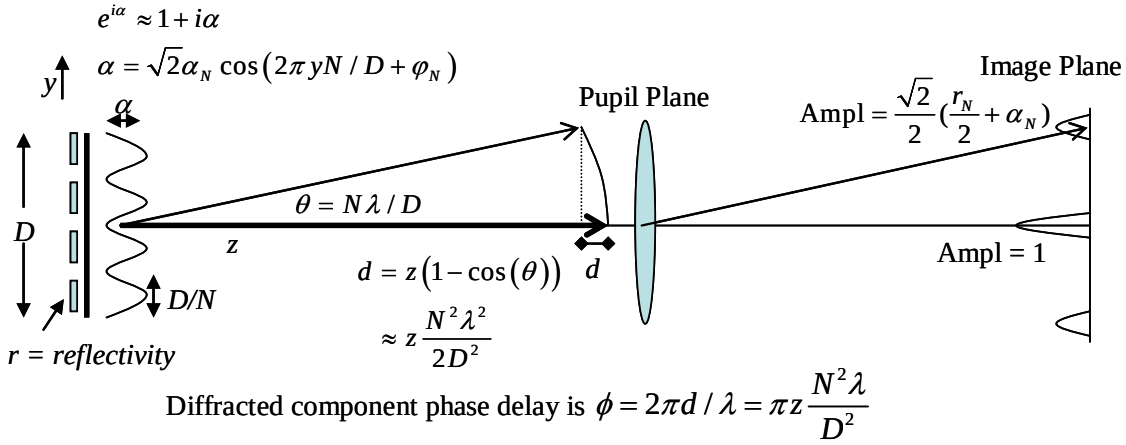

Figure 2. A beam with weak phase modulation α propagates along the *z*-axis. The diffracted beam has a phase delay ϕ relative to the main beam. The diffracted light propagates to a point spread function at an angle θ.

Table 1: Zero, First, and Second Order Propagation Terms

Perturbation	Name	Propagation	Effect	λ-Dependence	Michelson or VN	Sequential
Ampl. non-uniformity	$E_r = r/2$	no	Ampl.	0	Limits refl. PSD	Controlled
Phase (surface) to ampl.	$E_{s,p} = 4\pi^2 szN^2/D^2$	1st order	Ampl.	0	Limits surf. PSD	Controlled
Surface figure	$E_s = 4\pi s/\lambda$	no	Phase	1/λ	Controlled	Controlled
Phase to phase	$E_{s,p2} = 2\pi^3 sz^2\lambda N^4/D^4$	2nd order	Phase	λ		Limits surf. PSD
Ampl. to phase	$E_{r,p} = \pi rz\lambda N^2/2D^2$	1st order	Phase	λ		Limits refl. PSD

Table 1 summarizes the five important terms of Eq. 3. Two terms have no wavelength dependence, one term has 1/λ-dependence, and two terms have λ-dependence. This, in a nutshell is the problem. With only two DMs in the system (or, like the visible nuller, and independent phase and amplitude controller), we can not control all the wavelength dependencies in the system. Interestingly, Pueyo[12] has analyzed the case where an additional DM is added for each desired order of wavelength-dependence to be suppressed. His analysis shows that regardless of the number of DMs employed, the surface uniformity requirement imposed by the next-highest uncontrolled order of wavelength dependence limits the diameter of controlled spatial frequencies as we will see below for the 2-DM and VN cases.

3. WAVE FRONT CONTROL ARCHITECTURES

One proposed TPF-C wave front control configuration employs two DMs in a symmetric Michelson configuration first proposed by Littman[3]. This architecture (Fig. 3) allows independent control of phase and amplitude variations. Phase is controlled when the two DMs have identical piston, while amplitude is controlled (without affecting phase) when they have opposite pistons (one 'pushes' while the other 'pulls'). The system then controls both the phase and amplitude components of the wave front and clears out a dark hole that is symmetric about the optical axis. It can be shown[2] that the amplitude generated by the pair of DMs varies as $1/\lambda^2$.

In the sequential configuration, one DM is placed in the pupil (DM_p), while a second one, DM_{np}, is located a distance z_{DM} downstream. With one or more DMs located away from the pupil, we have a propagation lever that provides a

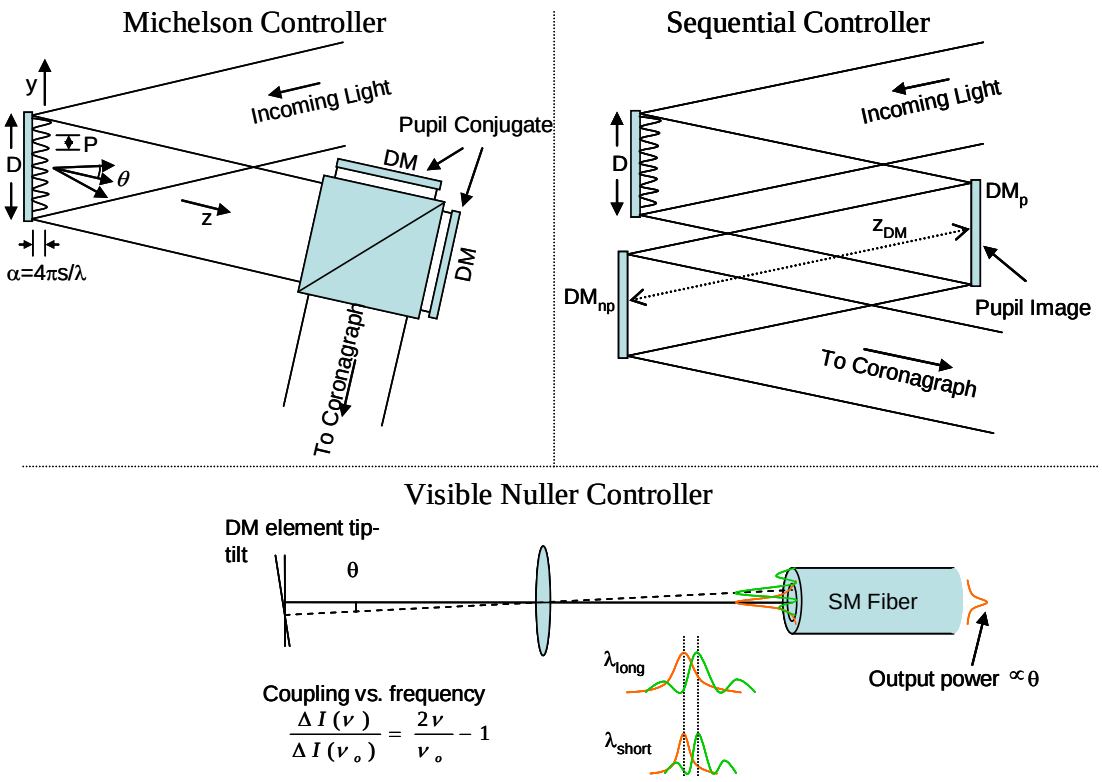

Figure 3. Wave front control systems. Upper left: In the Michelson controller, DMs move in opposite direction to control amplitude with 1/wavelength squared dependence.. Upper right: In the sequential configuration, a DM located some distance away from the pupil is actuated, resulting in wavelength-independent control in the pupil. In the visible nuller, tip-tilt actuators move a spot across the core of a single-mode fiber. Amplitude control varies as 1 / 2*wavelength.

wavelength-independent amplitude control term (the term $E_{s,p}$ in Eq. 3). DM_{np} is commanded to create a wavelength-independent amplitude that is a broad-band null of both E_r and the phase-to-amplitude term $E_{s,p}$ arising from other non-pupil optics. Alternatively, the two DMs could be located on either side of the pupil; as with the Michelson, the configuration provides independent phase and amplitude control.

A third approach is shown in the lower panel of Fig. 3. The visible nuller[4] (VN) is a coronagraph alternative proposed for TPF-C. It is a shearing interferometer followed by an array of lenslets mated to an array of single-mode (SM) fiber optics. The fiber optics serve as local spatial filters of the wave front. The DMs in the VN have segmented face sheets with one segment per lenslet. The segments have 3 degrees of freedom: piston for wave front phase control, and tip/tilt for amplitude control. The latter is achieved by tilting the beam so that the spot formed by the lenslet is offset relative to the core of the SM fiber. As shown in Figs. 3 and 4, this type of control is wavelength dependent. The diameter of the Airy spot grows linearly with wavelength, as does the dimension of the mode of the fiber Thus starlight-to-fiber coupling efficiency versus tilt is a function of wavelength, with longer wavelengths exhibiting less change in the output power for a given tilt than shorter wavelengths. The change in coupling at one wavelength relative to another is given by

$$\frac{\Delta I(\nu)}{\Delta I(\nu_o)} = \frac{2\nu}{\nu_o} - 1 \qquad . \tag{4}$$

Fig. 4 plots the results of a coupling calculation that verifies Eq. 4. The electric field follows the same law for small changes in coupling.

In summary, we have identified three wave front control configurations. All three control phase through surface deformation. This carries a $1/\lambda$ dependence as seen in the E_s term of Eq. 3. For amplitude control, the Michelson has $1/\lambda^2$ dependence, the Visible Nuller has $1/2\lambda$ dependence, and the sequential configuration is wavelength-independent.

4. BROAD BAND CONTRAST

Monochromatically, the DM configurations described in Sect. 3 can compensate the electric field terms in Table 1 and Eq. 3. However, in broad band light the DMs do not have enough degrees of freedom to perform broad band wave front compensation over the full dark hole. (They may be used to perform broad-band control of a subset of points but that is not the focus of this paper.) In our previous work[2] we derived surface figure and reflectivity uniformity requirements by limiting the leakage of light as a function of the spectral resolution, $R=\lambda/\Delta\lambda$, for the Michelson and sequential configurations. Here we will summarize the approach and previous results, then derive the leakage for the Visible Nuller.

Surface requirement for Michelson Configuration

We derive a surface figure requirement by considering how the Michelson configuration responds to the phase-induced-amplitude, $E_{s,p}$, arising from the propagation of phase corrugations from a non-pupil plane to the pupil plane. Table 1 shows that $E_{s,p}$ is wavelength independent. The Michelson amplitude control varies as $\lambda^{-2} = \nu^2/c^2$ where ν is the frequency of light and c is the speed of light. If we set the DMs to compensate $E_{s,p}$ at the center of the optical band, we can write the residual electric field as

$$E(\nu) = E_{s,p}\left(\left(\frac{\nu}{\nu_o}\right)^2 - 1\right) \qquad (5)$$

We next calculate the contrast, $C(\nu) = |E(\nu)|^2/2$, and integrate over optical frequency (because energy adds in equal increments of frequency) to obtain

$$\begin{aligned}\bar{C} &= \frac{1}{\Delta\nu} C_o \int_{\nu-\Delta\nu/2}^{\nu+\Delta\nu/2} \left(\left(\frac{\nu}{\nu_o}\right)^2 - 1\right)^2 d\nu \\ &= C_o\left(\frac{1}{80}\left(\frac{\Delta\nu}{\nu}\right)^4 + \frac{1}{3}\left(\frac{\Delta\nu}{\nu}\right)^2\right) \qquad (6) \\ &\approx \frac{C_o}{3R^2}\end{aligned}$$

where $C_o = |E_{s,p}|^2/2$. and R is the spectral resolution defined above. Substituting from Eq. 3 into Eq. 6, we find

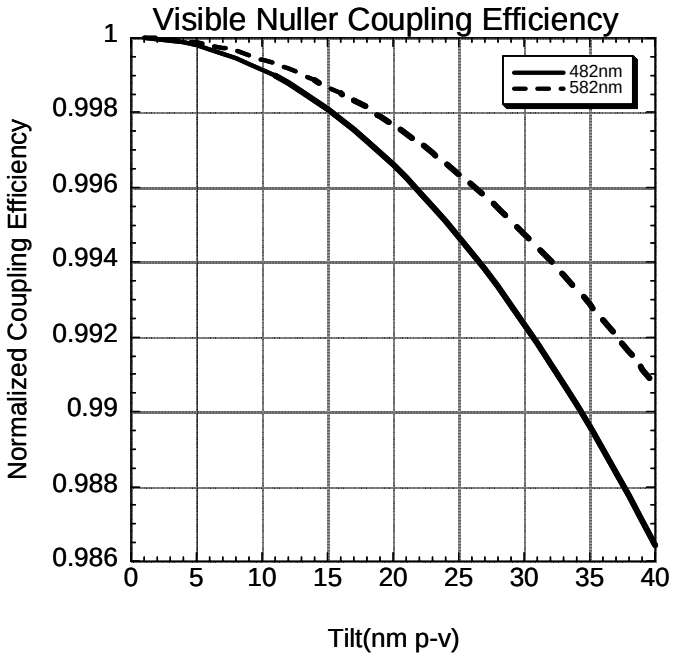

Figure 4. Visible Nuller coupling efficiency vs. tilt at two wavelengths. For a 1.1% drop in average coupling, the two wavelengths differ by 0.45%, a relative change of 41%. With $\Delta\lambda/\lambda$ = 100/532 = 19%, we find that the relative change of coupling across the band is twice the relative width of the band. This is consistent with eq. 4.

$$\bar{C} = \frac{1}{6R^2}\left(\frac{4\pi^2 szN^2}{D^2}\right)^2 \quad . \tag{7}$$

Given a contrast allocation, e.g. $\bar{C} = 10^{-12}$, we can solve for the r.m.s. surface height *s* at a given spatial frequency *N* cycles/aperture. For the current TPF-C optical design, we use *D*=10 cm and the distance *z* from reference 2 to derive the requirement on each optic. Note that optics with large propagation distances will have the tightest requirements. Eq. 7 does not yield requirement for the primary mirror since it has *z*=0. Fig. 5 shows the surface requirements for the Michelson configuration.

Reflectivity Requirement for Michelson Configuration

The reflectivity requirement is derived from the direct term E_r. Because this term does not involve propagation, it applies equally to all spatial frequencies. Following the procedure above, we find

$$r = 2\sqrt{6\bar{C}}R \quad . \tag{8}$$

For a mean contrast residual of $\bar{C} = 10^{-12}$, and a spectral bandwidth $\Delta\lambda$=100 nm at λ = 633 nm, we find r=3x10^{-5}. This is the r.m.s. reflectivity variation in a 1 cycle/aperture bandwidth, applied at any spatial frequency. The r.m.s. value for spatial frequencies of 1 to 100 cycles/aperture is then 3x10^{-3}. Reflectivity requirements are shown in Fig. 6.

Requirements for Visible Nuller Configuration

We now turn to the Visible Nuller which consists of two sequential nulling interferometers. Wave front control takes place in arm A of the first nuller. If nuller arm A has electric field E_o and arm B has electric field E_B=E_o + ΔE_o at the central frequency ν_o, the leakage is $C = |E_A - E_B|^2 = |\Delta E_o|^2$. The difference ΔE_o between arms is given by a combination of E_r and $E_{s,p}$, neither of which is wavelength-dependent. (Other terms will be present but these are the dominant ones that are not fully correctable by the wavelength-dependent fiber coupling approach.) For small changes to the intensity (e.g. the arms are almost matched, and a small DM tilt is required to slightly offset the sub-aperture image on the fiber tip), the change in the electric field is ½ the change in the intensity, while the relative change in electric field with wavelength is equal to the relative change in intensity, so that from Eq. 4 we have

$$\frac{\Delta E(\nu)}{\Delta E_o} = \frac{2\nu}{\nu_o} - 1 \tag{9}$$

The DM adjusts arm A so that at frequency ν_o, $\Delta E = 0$ and the contrast disappears. At a different frequency we have

$$\begin{aligned} C &= \left|\left(E_o + \Delta E_o\left(2\nu/\nu_o - 1\right)\right) - \left(E_o + \Delta E_o\right)\right|^2 / 2 \\ &= 2\left|\Delta E(\nu_o)\right|^2\left(\nu/\nu_o - 1\right)^2 \\ &= 4C_o\left(\nu/\nu_o - 1\right)^2 \end{aligned} \tag{10}$$

where we have again employed the relationship between contrast and electric field, $C_o = |\Delta E_o|^2 / 2$

Integrating over the bandpass to determine the average contrast, we find

$$\begin{aligned} \bar{C} &= \frac{4}{\Delta\nu} C_o \int_{\nu-\Delta\nu/2}^{\nu+\Delta\nu/2} \left(\frac{\nu}{\nu_o} - 1\right)^2 d\nu \quad . \\ &= \frac{C_o}{3R^2} \end{aligned} \tag{11}$$

We find that the Visible Nuller broadband contrast residual is the same as the Michelson residual. We thus conclude that the VN, assuming the same optics diameter and optical train characteristics, places the same requirements on the optics as the Michelson configuration (eqs. 7 and 8).

Our previous work[2] showed that the sequential configuration (SC) greatly relaxes the requirements, especially for reflectivity uniformity. The non-pupil DM in SC uses propagation to create amplitude variations in the pupil that are wavelength-independent – an $E_{s,p}$ term from the DM negates E_r. The term that limits reflectivity uniformity is then $E_{r,p}$, amplitude-induced-phase, which is proportional to λ. Because it arises from propagation, it is weaker than the 'direct' term E_r, leading to relaxed requirements on r.

We plot the surface and reflectivity requirements for the three wave front control configurations in Fig. 5. We also show how the requirements vary with spectral resolution, and compare the requirements to state-of-the art optics manufactured for EUV lithography[13]. The EUV optics are mounted, coated aspherics with 0.3 nm rms surfaces. We consider this to be the practical limit for optics that will fly on TPF

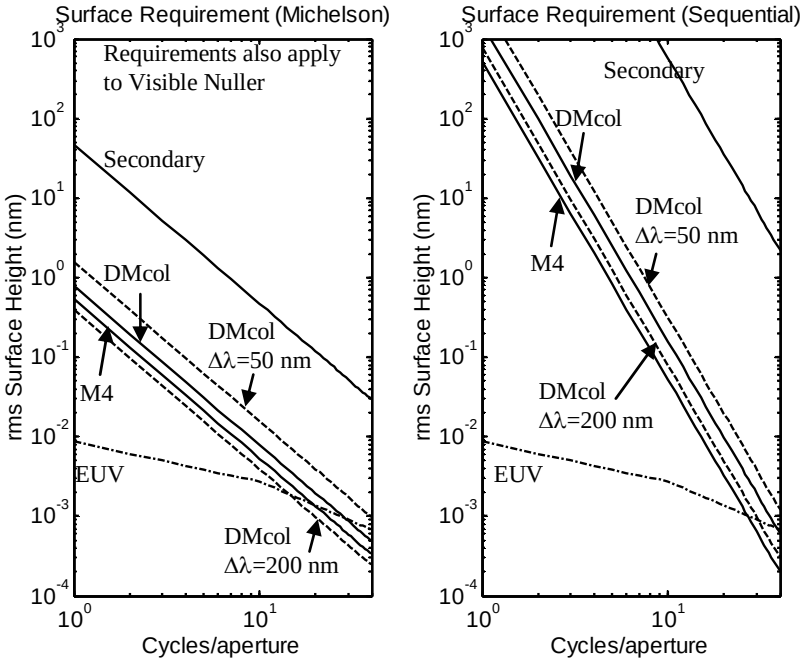

Figure 5. Surface figure requirements for Contrast = 10^{-12} for the Michelson, Visible Nuller, and sequential configurations. The curves all assume Δλ = 100 nm except otherwise indicated. The EUV curve is derived from a measured PSD and represents the state-of-the-art.

Fig. 5 shows that the DM collimator and M4 requirements exceed state-of-the-art EUV optics surfaces at ~ 20 cycles/aperture (Michelson and Visible Nuller) and ~30 cycles/aperture (sequential). The dashed curves show how the requirement depends on optical bandwidth. The Michelson / VN systems benefit more from bandwidth reduction and have about the same dark hole diameter as the sequential configuration for $\Delta\lambda$ = 50 nm. Conversely, at $\Delta\lambda$ = 200 nm, the Michelson/VN systems are limited to ~ 15 cycles/aperture.

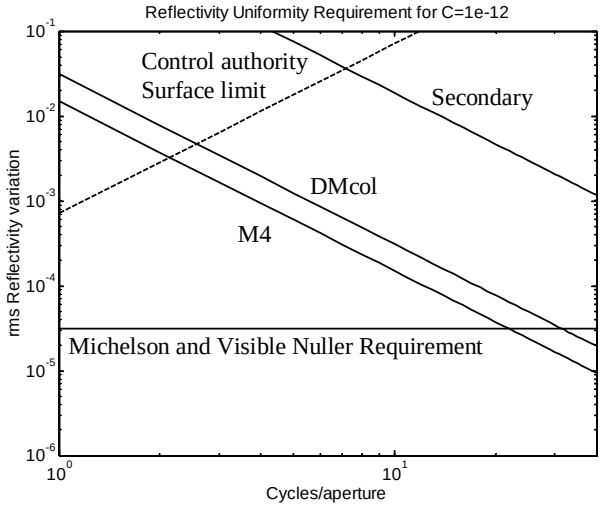

Figure 6. Surface figure requirements for C = 10^{-12} for the Michelson, VN, and sequential configurations. The Michelson and VN requirement is the horizontal line. The curves assume a 1 cycle/aperture bandwidth (= 1 speckle) and Δλ = 100 nm. Dashed line: amount reflectivity can change for a 30 nm piston of DM_{np} at a distance of 3 m from the pupil.

5. HIGH SPATIAL FREQUENCY FOLDING INTO THE DARK HOLE

We have to this point discussed surface spatial frequencies falling within the control bandwidth of the DM, that is spatial frequencies below *N/2* cycles/aperture, where the square DM has *N* elements per side. (Note: *N* was a free variable in Sections 2 and 3. We now treat it as a fixed value.)

For the VN, that is the end of the story because the SM fibers filter all spatial frequencies above N/2. For the other configurations light with higher spatial frequencies (e.g. *N*/2+5 and *N*/2+12 cycles/aperture) mixes together and folds into the dark hole (at 7 cycles/aperture in this example). Give'on et al (2006) refer to as 'frequency folding' and discuss optimal monochromatic control using band-limited DMs[14]. In broadband light, we must deal with the λ^{-2} wavelength dependence of the pure amplitude term arising from mixing of phase corrugations. Assuming the folded light can be sensed independently of other scattered light, it can be perfectly corrected by the Michelson with its λ^{-2} amplitude dependence, but not by the sequential configuration (wavelength-independent amplitude). Here we show how the effect arises and compute the residual field for the sequential configuration.

Consider a pupil of with clear aperture *A* and phase aberrations ϕ at wavelength λ. The electric field is given by $E(x) = Ae^{i\phi}$ with phase term

$$\phi = \sum_{m=0}^{\infty} \left(4\pi s_m / \lambda\right) \sin(2\pi x_m / D + \theta_m) \qquad (12)$$

Following Give'on et al (2006), we assume the surface errors $s_m << \lambda$ and we expand the field to second order to obtain

$$\begin{aligned} E(x) &\approx 1 + i\phi - \phi^2/2 \\ &= 1 + \sum_{m=0}^{\infty} \left(\frac{4\pi s_m}{\lambda}\right) \sin(2\pi x_m / D + \theta_m) - \frac{1}{2}\left(\frac{4\pi}{\lambda}\right)^2 \sum_{k=0}^{\infty}\sum_{m=0}^{\infty} s_m s_k \sin(2\pi x_m / D + \theta_m) \sin(2\pi \vec{x}_k / D + \theta_k) \end{aligned} \qquad (13)$$

We have dropped the pupil shape *A* from the equation for simplicity and note that in the image plane this term will convolve with the delta functions that are the Fourier Transforms of the sin() terms in Eq. 13. The convolution describes the shape of the 'speckles' formed by the forest of delta functions.

As discussed earlier, the coronagraph is designed to eliminate the constant term. Assuming an ideal DM and a means of sensing the second term independent of the others, the DMs cancel the second term up to *N*/2 by setting the DM surface height s_{DM} such that $s_{DM} = -s_m$ and $\theta_{DM} = \theta_m$. Once the DM is set to compensate the second term, the only light remaining inside the dark hole is the amplitude resulting from beating of the frequencies in the third term. We take the Fourier Transform (FT) of the third term (pure amplitude) and find that in the image plane we have

$$\begin{aligned} E_o(\xi) &= -\frac{1}{2}\left(\frac{4\pi}{\lambda}\right)^2 \sum_{k=N/2}^{\infty}\sum_{m=N/2}^{\infty} s_k s_m e^{i(\theta_k + \theta_m)} \left[\delta_\delta(\xi - m) * \delta_\delta(\xi - k)\right] \\ &= -\frac{1}{2}\left(\frac{4\pi\nu}{c}\right)^2 \sum_{k=N/2}^{\infty}\sum_{m=N/2}^{\infty} s_k s_m e^{i(\theta k + \theta_m)} \left[\delta\delta\left(\xi - (m-k)\right) + \delta\delta\left(\xi - (m+k)\right)\right] \end{aligned} \qquad (14)$$

where δ_δ is the FT of the sine function[15], $\delta\delta$ is the FT of the cosine function, * is the convolution function, and ξ is the image plane coordinate.

We are only concerned with energy appearing within the dark hole. This energy comes from the frequency folding terms $|m-k| < N/2$ in Eq. 14. The other terms $m+k$ scatter light outside the dark hole and will be dropped from further consideration. As noted earlier, the frequency folding term has λ^{-2} wavelength dependence.

Compensation in the Sequential Configuration

The sequential DM configuration introduces amplitude modulation in the pupil via propagation of phase modulation at the non-pupil DM. In Eq. 3 we showed that for a periodic surface height function s_A on the non-pupil DM located a distance z_{DM} from the pupil, the phase-induced-amplitude in the pupil is

$$E_{sq}(x) = \frac{4\pi^2 s_A(x) z_{DM} N^2}{D^2} \qquad (15)$$

The wavelength-independent image plane field, $E_{sq}(\xi)$ perfectly compensates the frequency folding field at λ_o if we select s_A such that $E_{sq} = E_o$, but does not cancel it over a broad band. The residual field after compensation is

$$\begin{aligned} E(\xi,\nu) &= E_o(\xi)\left(\frac{\nu}{\nu_o}\right)^2 - E_{sq}(\xi) \\ &= E_o(\xi)\left(\left(\frac{\nu}{\nu_o}\right)^2 - 1\right) \end{aligned} \tag{16}$$

The residual contrast in the image plane is given by

$$C(\xi,\nu) = \left|\frac{E_o}{2}\left(\left(\frac{\nu}{\nu_o}\right)^2 - 1\right)\right|^2 = C_o(\xi)\left(\left(\frac{\nu}{\nu_o}\right)^2 - 1\right)^2 \tag{17}$$

where $C_o(\xi) = \left|E_o(\xi)\right|^2 / 2$ is the uncompensated contrast due to frequency folding. This equation is of the same form as Eq. 5 allowing us to immediately determine that the average residual compensation over a bandpass $\Delta\nu$ is given by

$$\begin{aligned} \bar{C}(\xi) &= \frac{1}{\Delta\nu} C_o(\xi) \int_{\nu-\Delta\nu/2}^{\nu+\Delta\nu/2} \left(\left(\frac{\nu}{\nu_o}\right)^2 - 1\right)^2 d\nu \\ &\approx \frac{C_o(\xi)}{3R^2} \end{aligned} . \tag{18}$$

We desire to express the residual contrast in terms of the PSD of the optics. To do this, we evaluate the expectation of the contrast term, substituting from Eq. 14 into Eq. 18 to obtain

$$\left\langle \bar{C}(\xi) \right\rangle = \frac{1}{6R^2}\left(\frac{4\pi}{\lambda_o}\right)^4 \left\langle \left| \sum_{k=N/2}^{\infty} \sum_{m=N/2}^{\infty} s_k s_m e^{i(\theta_k+\theta_m)} \delta\delta\left(\xi - (m-k)\right) \right|^2 \right\rangle \tag{19}$$

We assume that the spatial frequencies across the optics are all uncorrelated, so that $\langle s_m s_k \rangle = 0$ $(m \neq k)$ and $\left\langle s_m^2 \right\rangle = \sigma_m^2$ is the variance of the surface height at a frequency *m* cycles/aperture. The surface variance in a spatial bandwidth *dk* cycles/m is related to the surface Power Spectral Density (PSD) by

$$\sigma_m^2 = \frac{PSD(k)}{dk \cdot dk} \tag{20}$$

We then have

$$\left\langle \bar{C}(\xi) \right\rangle = \frac{1}{6R^2}\left(\frac{4\pi}{\lambda_o}\right)^4 \sum_{n=N/2}^{\infty}\sum_{m=N/2}^{\infty} \sigma_n^2 \sigma_m^2 \delta\delta\left(\xi - (m-n)\right)$$
$$= \frac{1}{6R^2}\left(\frac{4\pi}{dk\lambda_o}\right)^4 \sum_{m=N/2}^{\infty} PSD_m PSD_{m+\xi} \qquad (21)$$

For convenience in notation we have written the convolution as a one-dimensional quantity. However, the sum is performed over the 2-dimensional overlap of the circularly symmetric PSD functions. We can arrive at the same formulation using the wave front expansion of Perrin et al (2003)[16].

The results of high-frequency folding for two large optics – a Very Large Telescope (VLT) primary mirror and the Hubble Space Telescope (HST) primary mirror – are shown in Fig. 7. Data for the PSD of these optics is taken from Borde & Traub (2006)[17]. Surprisingly the VLT mirror at high-spatial frequencies is a very good surface, with just a 4 nm r.m.s. surface above 40 cycles/aperture. If this telescope were used uncompensated in TPF-C, the frequency folding contrast would be 10^{-11}. After compensation at the central frequency of a 100 nm bandpass, the contrast in the sequential DM configuration is ~ 10^{-13}. This is acceptable and shows that current technology produces 8-m optics with PSDs that meet the TPF-C high-spatial frequency requirements.

6. CONCLUSIONS

This work shows that for spatial frequencies up to ~ 30 cycles/aperture, and for frequencies above the DM Nyquist cutoff (~ 50 cycles/aperture), the optical surface requirements can be met within the existing state-of-the-art (SOA). Reflectivity requirements look readily achievable as well. However, in the range > 30 cycles/aperture (> 20 cy/aperture for the VN and Michelson configurations), the wavelength dependence of propagation effects demands that the optical surfaces be far superior to SOA EUV optics. It is highly unlikely that coated, mounted surfaces of this quality can be produced. Our curves in Fig. 5 show that reducing the optical bandwidth broadens the dark hole, but of course this brings reduced sensitivity. Fortunately, the vast majority of terrestrial planets detectable with TPF-C fall within the useful part of the dark hole. The detection of Jovian planets will be impacted, however.

This work was carried out at the Jet Propulsion Laboratory, California Institute of Technology, under contract with the National Aeronautics and Space Administration.

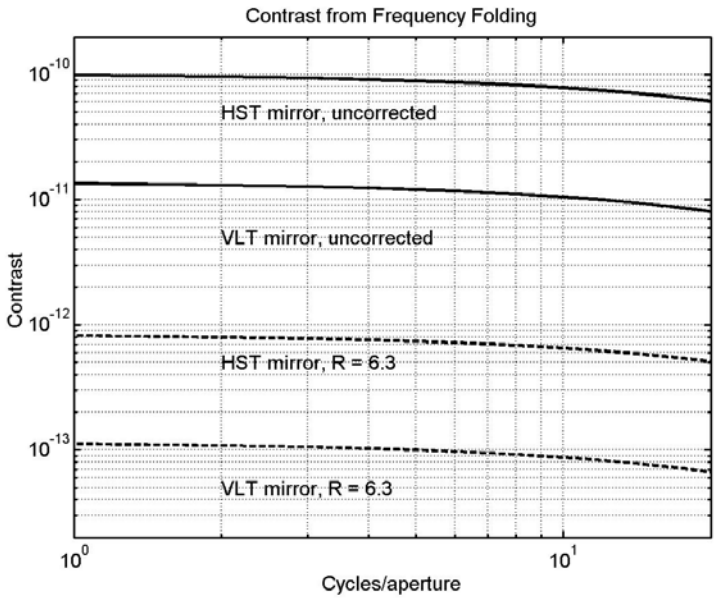

Figure 7. Contrast from frequency folding for spatial frequencies above 48 cycles per aperture, for an 8-m VLT primary and the 2.4 m HST primary. The uncompensated effect is above the required level of 10^{-12} for both mirrors. The sequential DM configuration provides about ~100x reduction of the contrast when it compensates the center of a 100 nm bandpass centered at 633 nm. Both mirrors are acceptable after compensation. The frequency folding effect can be perfectly compensated by the Michelson configuration and is not present in the Visible Nuller.

REFERENCES

1. V.G. Ford, et al, "The Terrestrial Planet Finder Coronagraph Technology and Mission Design Studies," Proc. SPIE Vol. **5487**, 1274-1283 (2004).
2. S. B. Shaklan & J. J. Green, "Reflectivity and Optical Surface Height Requirements in a Broad-band Coronagraph 1: Contrast Floor Due to Controllable Spatial Frequencies," accepted for publication in Applied Optics (2006).
3. M.G. Littman, M. Carr, J. Leighton, E. Burke, D. N. Spergel, and N. J. Kasdin, "Phase and amplitude control ability using spatial light modulation and zero path length difference Michelson interferometer," Proc. SPIE **4854**, 405-412 (2003).
4. B. P. Mennesson et al, "Optical Planet Discoverer: How to Turn a 1.5m Class Space Telescope into a Powerful Exo-planetary Systems Imager," Proc. SPIE **4860**, 32-44 (2003).
5. R. A. Brown, "Single-Visit Photometric and Obscurational Completeness," ApJ **624**, 1010-1024 (2005).
6. M. A. Ealey and J. T. Trauger, "High density deformable mirrors to enable coronagraphic planet detection," Proc. SPIE **5166**, 172-179 (2004).
7. Trauger, J.T., et al, "Coronagraph Contrast Demonstrations with the High Contrast Imaging Testbed," Proc. SPIE Vol. **5487**, pp. 1330-1337 (2004).
8. Kuchner, M.J., and Traub, W.A., "A Coronagraph with a Band-Limited Mask for Finding Terrestrial Planets," ApJ **570**, pp. 900-908 (2002).
9. N. J. Kasdin et al, "Extrasolar Planet Finding Via Optimal Apodized-Pupil and Shaped-Pupil Coronagraphs," ApJ **582**, 1147-1163 (2003).
10. O. Guyon et al, "Exoplanet Imaging with a Phase-induced Amplitude Apodization Coronagraph. I. Principle," ApJ **622**, 744-758 (2005).
11. D. M. Palacios, "An Optical Vortex Coronagraph," Proc. SPIE **5905**, 196-205 (2005).
12. L. A. Pueyo et al, "Wavelength Dependence of Aberrations in the Near Field: Influence and Compensation of Fresnel Effects in Coronagraphs," Proc. SPIE **6265** (this conference, 2006).
13. J. S. Taylor, "Progress in meeting stringent optical system requirements in EUV lithography," presented at SPIE's 26th Symposium on Microlithography and Emerging Lithographies V, Santa Clara, CA, 25 Feb.– 2 March, 2001
14. A. Give'on et al, "On Representing and Correcting Wavefront Errors in High-Contrast Imaging Systems," JOSA-A **23**, 1063-1073 (2006).
15. J. D. Gaskill, *Linear System, Fourier Transforms, and Optics* (Wiley & Sons, 1978).
16. M. D. Perrin et al, "The Structure of High Strehl Ratio Point-Spread Functions," ApJ **596** 702-712 (2003).
17. P. J. Borde & W. A. Traub, "High-Contrast Imaging from Space: Speckle Nulling in a Low-Aberration Regime," ApJ **638**, 488-498 (2006).